# Structural reorganization of the antigen-binding groove of human CD1b for presentation of mycobacterial sulfoglycolipids

Luis F. Garcia-Alles[a,b,1], Anthony Collmann[c], Cees Versluis[d], Buko Lindner[e], Julie Guiard[a,b], Laurent Maveyraud[a,b], Emilie Huc[a,b], Jin S. Im[f], Sebastiano Sansano[c], Thérèse Brando[a,b], Sylviane Julien[a,b], Jacques Prandi[a,b], Martine Gilleron[a,b], Steven A. Porcelli[f], Henri de la Salle[g,h,i], Albert J. R. Heck[d], Lucia Mori[c,j], Germain Puzo[a,b], Lionel Mourey[a,b,1], and Gennaro De Libero[c,1]

[a]Centre National de la Recherche Scientifique, Institut de Pharmacologie et de Biologie Structurale, F-31077 Toulouse, France ; [b]Université de Toulouse, Université Paul Sabatier, Institut de Pharmacologie et de Biologie Structurale, F-31077 Toulouse, France; [c]Experimental Immunology, Department of Biomedicine, Basel University Hospital, CH-4031 Basel, Switzerland; [d]Biomolecular Mass Spectrometry and Proteomics Group, Bijvoet Center for Biomolecular Research and Utrecht Institute for Pharmaceutical Sciences, Utrecht University, and Netherlands Proteomics Centre, 3584 CH, Utrecht, The Netherlands; [e]Division of Immunochemistry, Research Center Borstel, D-23845 Borstel, Germany; [f]Department of Microbiology and Immunology, Albert Einstein College of Medicine, Bronx, NY 10461; [g]Biology of Human Dendritic Cells, Institut National de la Santé et de la Recherche Médicale, Unité Mixte de Recherche S725, F-67065 Strasbourg, France; [h]Université de Strasbourg, F-67000 Strasbourg, France; [i]Etablissement Français du Sang-Alsace, F-67065 Strasbourg, France; and [j]Singapore Immunology Network, Agency for Science Technology and Research, Biopolis 138648, Singapore

Edited by Peter Cresswell, Yale University School of Medicine, New Haven, CT, and approved September 23, 2011 (received for review June 24, 2011)

**The mechanisms permitting nonpolymorphic CD1 molecules to present lipid antigens that differ considerably in polar head and aliphatic tails remain elusive. It is also unclear why hydrophobic motifs in the aliphatic tails of some antigens, which presumably embed inside CD1 pockets, contribute to determinants for T-cell recognition. The 1.9-Å crystal structure of an active complex of CD1b and a mycobacterial diacylsulfoglycolipid presented here provides some clues. Upon antigen binding, endogenous spacers of CD1b, which consist of a mixture of diradylglycerols, moved considerably within the lipid-binding groove. Spacer displacement was accompanied by F′ pocket closure and an extensive rearrangement of residues exposed to T-cell receptors. Such structural reorganization resulted in reduction of the A′ pocket capacity and led to incomplete embedding of the methyl-ramified portion of the phthioceranoyl chain of the antigen, explaining why such hydrophobic motifs are critical for T-cell receptor recognition. Mutagenesis experiments supported the functional importance of the observed structural alterations for T-cell stimulation. Overall, our data delineate a complex molecular mechanism combining spacer repositioning and ligand-induced conformational changes that, together with pocket intricacy, endows CD1b with the required molecular plasticity to present a broad range of structurally diverse antigens.**

three-dimensional structure | groove shrinking | diacylglycerol endogenous ligand | T lymphocyte activation | CD1b mutant transfectant

T lymphocytes have developed the capacity to recognize as antigens a large variety of molecules including peptides, (glyco)lipids, and phosphorylated metabolites (1). Specific recognition of peptides or lipids by T-cell receptors (TCR) occurs when these molecules form antigenic complexes with dedicated antigen-presenting molecules belonging to MHC or CD1 families, respectively. Diversity has forced the immune system to develop appropriate strategies to present antigens in immunogenic form. Polymorphic MHC molecules cope with the peptide repertoire by constraining the ligand conformational space (2). Less clear is how the immune system adapts to the large glycolipid antigenic range and forms antigenic complexes using the functionally nonpolymorphic CD1 molecules.

Human antigen-presenting cells (APC) display the CD1a, CD1b, CD1c, and CD1d proteins on their plasma membranes (1, 3). CD1 ectodomains consist of a heavy chain, which folds into three extracellular domains (α1–α3) noncovalently associated with β2-microglobulin (4). Antigen-binding grooves nestle between the α1 and α2 domains and are mostly lined by hydrophobic residues. This allows the antigenic lipids to be anchored via their hydrophobic chains, so that polar motifs protrude toward the aqueous milieu. Consequently, polar heads but not hydrophobic tails are assumed to establish stimulatory contacts with TCRs. Nevertheless, modifications in the lipid chains may also indirectly impact on TCR recognition (5).

The number, shape, and connectivity of pockets vary among CD1 molecules. CD1b has the most voluminous and intricate groove, being composed of A′, C′, and F′ pockets and a T′ tunnel that interconnects the deep ends of A′ and F′ pockets (6). In agreement with groove structural complexity, human CD1b presents the greatest diversity of antigenic structures among CD1 proteins, including mycobacterial lipoarabinomannans and phosphatidylinositol mannosides (7–9), diacylsulfoglycolipids ($Ac_2SGL$) (10), mycolic acids (MA) (11), glucose- and glycerol-monomycolates (GMM and GroMM, respectively) (12, 13), and self-lipids such as GM1 gangliosides (14) and sulfatides (15). The polar heads of these antigens vary in size from the small carboxylic group of MA to the pentasaccharide of GM1 or potentially larger structures in lipoarabinomannans. Hydrophobic tails, which decisively govern CD1-restricted presentation of some antigens (16, 17), also greatly differ in length and structural complexity. For example, up to $C_{80}$ long tails, which are not trimmed before presentation (18), compose MA and GMM, whereas short 18:1/16:0 tails are found in GM1.

*Mycobacterium tuberculosis* (*Mtb*) $Ac_2SGL$ lipids are known to stimulate specific T cells from *Mtb*-infected donors (10) and therefore are good candidate for novel lipid-based vaccines. Herein, we investigated how CD1b generates T-cell–stimulatory complexes with a synthetic sulfoglycolipid analog of $Ac_2SGL$. Our study clarifies how CD1b copes with antigens of variable tail length and complexity and why in some cases T cells are strongly sensitive to the structure of antigen hydrophobic tails. These findings are relevant for the development of new-generation subunit vaccines.

Author contributions: L.F.G.-A. and G.D.L. designed research; L.F.G.-A., A.C., C.V., B.L., E.H., T.B., S.J., L. Mori, and L. Mourey performed research; J.G., J.S.I., S.S., J.P., M.G., S.A.P., H.d.l.S., L. Mori, G.P., and G.D.L. contributed new reagents/analytic tools; L.F.G.-A., A.C., C.V., B.L., L. Maveyraud, A.J.R.H., L. Mori, G.P., L. Mourey, and G.D.L. analyzed data; and L.F.G.-A. and G.D.L. wrote the paper.

The authors declare no conflict of interest.

This article is a PNAS Direct Submission.

Data deposition: The atomic coordinates and structure factors reported in this paper have been deposited in the Protein Data Bank, http://www.rcsb.org (PDB ID 3T8X).

[1]To whom correspondence may be addressed. E-mail: alles@ipbs.fr, Lionel.Mourey@ipbs.fr, or Gennaro.DeLibero@unibas.ch.

This article contains supporting information online at www.pnas.org/lookup/suppl/doi:10.1073/pnas.1110118108/-/DCSupplemental.

## Results

**Stimulation of Specific T Cells by shCD1b Loaded in Vitro with $Ac_2SGL$ or SGL12.** In the present study we investigated the structural and functional characteristics of native recombinant soluble human CD1b (shCD1b, expressed from mammalian cells) in complex with the $Ac_2SGL$ antigen or the synthetic analog SGL12 (Fig. S1*A*). Complex formation was confirmed by isoelectric focusing (IEF) (Fig. S1*B* and ref. 17) and found to be optimal at pH 4.0 (Fig. S1*C*), in agreement with previous findings proving that presentation requires CD1b and $Ac_2SGL$ to encounter in acidic compartments of living APC (10). Importantly, plate-bound shCD1b–SGL12 elicited strong cytokine release from $Ac_2SGL$-specific T cells (Fig. S1*D*). These experiments also confirmed the antigen specificity, the CD1b restriction of the T-cell response, and ruled out potential effects of the CD1b-expression system (Fig. S1 *D–F*).

**Stimulatory shCD1b–SGL12 Complex Contains an Endogenous Spacer.** Immunogenic shCD1b–antigen complexes were characterized by native mass spectrometry (n-MS) (19), an approach that permitted identification of phosphatidylcholine (PC) and a spacer molecule (UL) as major endogenous ligands associated to shCD1b (20). We focused on complexes with SGL12, because naturally occurring $Ac_2SGL$ is molecularly heterogeneous in fatty acids linked at positions 2 and 3 of the sulfotrehalose (Fig. S1*A*). To further facilitate the interpretation of MS data, shCD1b–SGL12 was enriched by chromatofocusing.

In positive-ion mode electrospray ionization (ESI) n-MS, the mass of the major species observed for fully glycosylated shCD1b–SGL12 (Fig. 1*A*, black line) supported the association of SGL12 (1,064 Da) with ligand-free shCD1b (major species with unloaded shCD1b; Fig. 1*B*, black line). The shCD1b–SGL12 species nearly disappeared when the desolvation energy was reduced, and a peak that suggested simultaneous UL presence emerged (Fig. 1*A*, gray line). The presence of shCD1b–SGL12–UL in solution was supported by the negative-ion mode ESI data. Thus, whereas ligand-free shCD1b was detected as major species (Fig. 1*C*, black line), a broad peak was again observed at lower desolvation energy (Fig. 1*C*, gray line). The higher than expected weight of this species is likely due to unspecific binding of water and buffer molecules onto the gas phase ions at low energies (21).

Tandem MS-MS studies helped to corroborate the identity of the shCD1b–SGL12–UL species. Subjecting the presumed shCD1b–SGL12–$UL^{14+}$ pseudomolecular ions to collision-induced dissociation led to the precursor ion (indicated by an asterisk in Fig. 1*D*) and to two peaks indicative of dissociation of 600- to 640-Da ligands, which were directly detected in the low *m/z* region (Fig. 1*D*, *Inset*). In these experiments, dissociation of the anionic SGL12 was likely prevented by the tight interaction

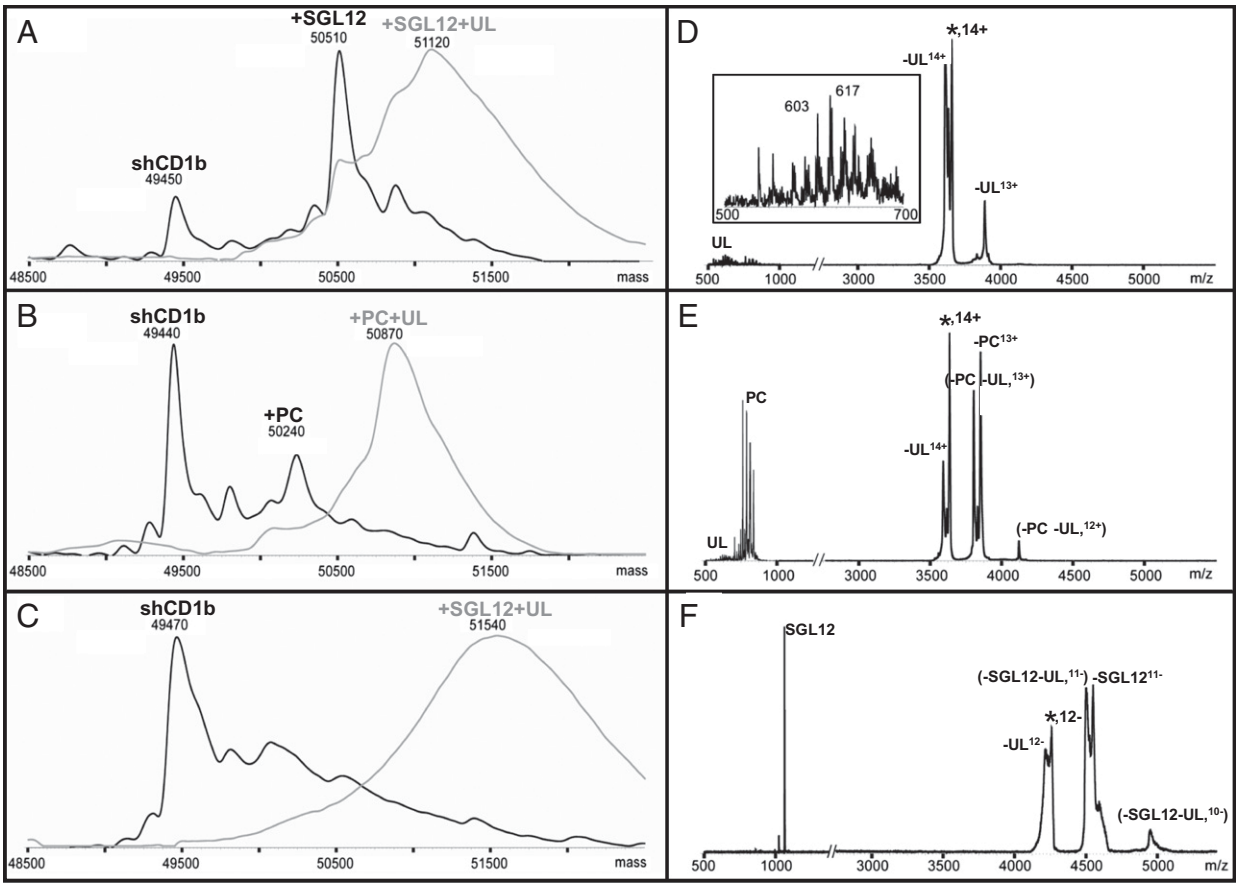


**Fig. 1.** Presence of combined SGL12 and endogenous spacer in stimulatory complexes. Neutral mass spectra obtained after averaging over all charged states the positive- (*A* and *B*) and negative-ion mode (*C*) ESI-MS native data. Spectra are from fully glycosylated shCD1b after incubation with SGL12 (*A* and *C*) or before addition of any lipid (*B*). Spectra recorded using harsh or low desolvation energies are drawn with black or gray lines, respectively. (*D–F*) Tandem MS-MS data recorded after selection of 14+ (*D* and *E*) or 12- (*F*) precursor ions corresponding to the most abundant species detected at low desolvation energies in *A* and *B* or *C*, respectively. Ligand dissociation from precursor ions (indicated with an asterisk) lead to appearance of additional protein peaks in the high-mass range. In addition, these ligands could be directly detected in the low-mass range, provided that the ligand charge is compatible with the ion mode detection. The 500- to 1,000-Da mass region of *D* and *E* is 20-fold enlarged on the *y* axis and 200-fold enlarged for *Inset* in *D*. The faint PC signals observed in *D* are attributed to <5% contaminant shCD1b–PC–UL.

with the positively charged protein surface. Definitive proof for the simultaneous presence of SGL12 was attained when the shCD1b–SGL12–$UL^{12-}$ ions were subjected to tandem MS-MS. The precursor ion decomposed by loss of approximately 1,070 Da and a negative charge (-SGL12; Fig. 1*F*). Additional signals arose from neutral loss of *ca.* 550 Da (-UL) or a simultaneous loss of approximately 1,600 Da (-SGL12 -UL). Further supporting the presence of SGL12, its molecular ion was observed in the low *m/z* region of the spectrum, whereas no signal attributable to UL was detected.

**Identification of the Spacer Lipid.** Weak signal intensities and the difficulties to fragment UL species dissociating from shCD1b impeded their characterization by n-MS. We then attempted the characterization of protein extracts by Fourier transform ion cyclotron resonance (FT-ICR) MS, a technique that could permit direct attribution of molecular formula from mass values. UL species could be recovered in petroleum ether (PE) after complete digestion of shCD1b with proteinase K, whereas PC was mostly found in subsequent extractions with chloroform. UL signals were detected in positive-ion mode ESI FT-ICR MS (Fig. S2*A*), at *m/z* values matching well those observed for species that dissociate from shCD1b in n-MS experiments (Fig. 1*D* and Fig. S2*B*). Relative intensities varied notably between the two spectra. This was attributed to instrumentation effects (see below), because data obtained by n-MS on the PE extract resembled closely the spectra recorded from shCD1b (compare Fig. S2 *B* and *C*).

Elemental composition analysis permitted grouping of UL species detected by FT-ICR MS as belonging to three families. First-group masses invariantly furnished as best hit $C_{35–43}H_{67–73}O_3$ molecular formula (Table S1, in plain black letters). For the second family, masses matched within the instrument accuracy (<3 ppm) to $C_{35–43}H_{65–75}O_4$ formula (Table S1, bold black letters). Some of these masses also fitted to $C_xH_yO_4Na^+$ or $C_xH_yO_3Li^+$ adducts. Conversely, hits with four or six nitrogen atoms (e.g., $C_{38}H_{68}N_4Na$ for *m/z* 603.5341 species) were ruled out because unprecedented in the literature and in public lipid databases. Finally, two peaks were assigned to $C_{37–39}H_{70–72}O_5Na$ (Table S1 in gray), suggesting diacylglycerol sodium adducts (diAcGro).

With the exception of a few $C_xH_yO_3Li^+$ hits, all species in Table S1 furnished formula with odd carbon atom number. We interpreted this as indicative of the presence of glycerol-based moieties ($C_3$). Extracted UL species continued to be reluctant to fragmentation in tandem MS experiments. Exploitable data could only be obtained for the species at *m/z* 603.5 (Fig. S2*D*), which furnished almost identical spectra to those obtained after selection of the *m/z* 603.5 signal present in commercial triolein, which arises from elimination of a single oleic acid (Fig. S2*E*).

Major UL species migrated on silica TLC plates comparably to synthetic diradylglycerols and were more retained than wax esters (i.e., stearyl-stearate) (Fig. S2*F*). The retention factor ($R_f$) of the most abundant species revealed with a $CuSO_4$ universal reagent was compatible with alkylacylglycerols (AkAcGro) and diAcGro. Although FT-ICR MS species intensities suggested that diAcGro ($C_xH_yO_5Na^+$ adducts) could be less abundant, experiments with synthetic AkAcGro and diAcGro indicated that $[M+H-H_2O]^+$ dehydration peaks could become prominent under FT-ICR MS conditions but not in n-MS experiments. Accordingly, $C_xH_yO_3$ and $C_xH_yO_4$ species of Fig. S2*A* could arise from $C_xH_{y+2}O_4$ (AkAcGro) and $C_xH_{y+2}O_5$ (diAcGro) species, as proposed in Table S1. To clarify this point, a $^1H$ NMR spectrum was recorded overnight on a PE-extracted UL sample and compared with a control sample (Fig. S2*G*, *Top* vs. *Middle*). Signals in the 2.2- to 5.2-ppm interval supported that UL mostly consisted of a mixture of 1,2- and 1,3-regioisomers of AkAcGro and diAcGro. Indeed, the UL spectrum closely resembled the $^1H$-NMR data recorded for a mixture of synthetic AkAcGro and diAcGro. Of note, such diradylglycerol structures are fully compatible with the linear electron densities attributed to UL in high-resolution structures of shCD1b (ref. 20 and below).

**Determination of the Structure of the CD1b–SGL12–Spacer Complex.** MS experiments identified shCD1b–SGL12–UL with 1:1:1 stoichiometry as the T-cell stimulatory complex. To clarify how diacylsulfoglycolipid presentation to T cells is compatible with the presence of UL, a strongly stimulatory sample containing fully glycosylated shCD1b loaded to approximately 75% occupancy with SGL12 was crystallized, and the structure was solved at a resolution of 1.90 Å (Table S2). Two molecules (copy A and B) were found per crystallographic asymmetric unit. All main structural features were similar for both molecules (rmsd of 0.40 Å on backbone atoms) and were common to published CD1b structures (6, 20, 22). The C′ portal was closed in both copies.

SGL12 was unequivocally identified in copy A (Fig. 2*A*). Electron density consistent with the sulfotrehalose polar head and disconnected stretches of the lipid tails was present in this copy from the earliest electron density maps. Conversely, weak electron density was found at the same relative location in the second copy (Fig. 2*B*), suggesting low SGL12 pocket occupancy. For that reason, the polar head for this second copy was omitted from the final structure. Extra electron density indicative of spacers presence was also found filling the T′ channel and the F′ pocket in both copies (Fig. 2*A*). The species and length heterogeneity of spacers and the impossibility of predicting its insertion orientation within the groove led us to build into such electron density a $C_{40}$-long carbon chain representative for the average length of diradylGro species.

The electron density of the SGL12 sulfotrehalose head in copy A connected during refinement to the electron density tube present in the C′ pocket but not with those extending downward to the A′ or F′ pockets. Nonetheless, such lack of connectivity was not a source of structural ambiguity concerning the lipid insertion mode, because the structural constraints imposed by the well-defined sulfotrehalose head dictated an unequivocal arrangement with the palmitic acid in the C′ pocket and the phthioceranoyl-like tail in the A′ pocket. The gap of electron density between the A′ entrance and the polar head corresponded to the tetramethyl-branched portion of the fatty acid tail that esterifies position 3 of SGL12 (Fig. S1*A*). This hydrophobic patch is located in an unfavorable water-exposed environment that must prevent the establishment of a privileged conformation. In addition, its emplacement at the entrance of the A′ pocket must fluctuate depending on the length heterogeneity of accompanying spacer molecules. These two factors might explain the poor definition in the electron density map for this patch.

**Polar Head Exposure and Positioning Above the Groove.** Hydrogen bonds between the guanidinium group of Arg79 and the 3′- and 4’-OH groups of the sulfated glucose stabilized in copy A the SGL12 polar head in a conformation that may favor the interaction of the sulfate with the TCR (Fig. 2*C*), in agreement with its essential role in T-cell activation (10). Arg79 is conserved in CD1b and CD1d of other species and plays a key ligand-binding role in CD1d structures (23–25). However, unlike CD1d, which often holds lipid polar heads by establishing hydrogen bond interactions with several residues (23–28), no further direct polar head-anchoring residues were found in the SGL12-loaded CD1b structure. The interaction between the SGL12 sulfotrehalose and Arg79 was solely reinforced by indirect hydrogen bonds, mediated by water molecules, with Gly76 and Gln152.

Polar heads are usually weakly defined in 3D structures of CD1b–lipid complexes (6, 20, 22). In relation to this, the SGL12 sulfotrehalose is *ca.* 3 and 10 Å more elevated above the pocket main portal than, for instance, the galactosyl rings of αGalCer and sulfatides bound to CD1d (27) and CD1a (29), respectively. Taken together, these data indicate that CD1b weakly interacts with

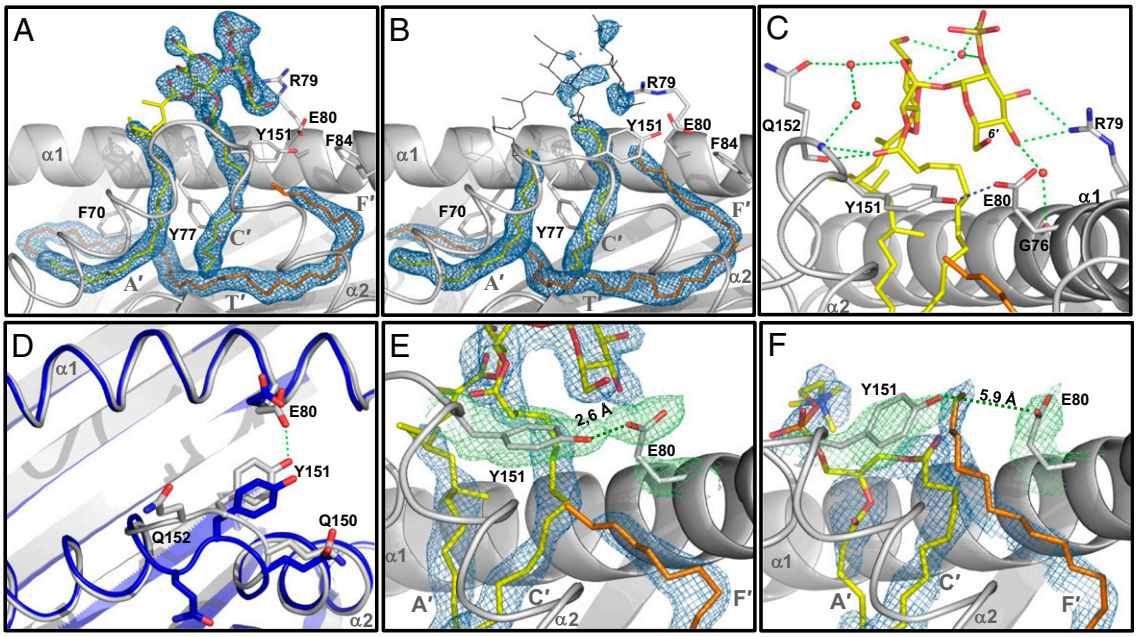


**Fig. 2.** Ligand binding and pocket alterations in shCD1b–SGL12–UL. (*A*) Electron density for the SGL12 and spacers in copy A (final $2F_o$-$F_c$ map contoured at 1.0 σ, blue mesh). Modeled lipids are drawn as sticks. SGL12 is colored by atom type (carbon yellow, oxygen red, sulfur orange), spacer in orange. The α2 domain helices are represented as thin ribbons. Gray letters indicate the groove channels occupied by nearby portions of electron density. (*B*) Electron density in the lipid-binding groove for copy B. Only ligand portions shown as yellow or orange sticks were modeled. For comparison, a full SGL12 molecule in the conformation observed in copy A (black lines) is superimposed onto the groove of copy B. (*C*) Hydrogen bonds established between SGL12 and CD1b. Hydrogen bonds between the lipid and Arg79 or Gln152, as well as indirect interactions mediated by water molecules (red spheres) with Gln152 and Gly76, are depicted as green dashed lines. (*D*) Comparison of the conformation adopted by residues from the α1-α2 domains of shCD1b–SGL12–UL (copy A, in gray) with those from shCD1b–PC–UL (20) (Protein Data Bank entry 2H26, in blue), after superimposition of backbone atoms of residues 6–180 from each structure. For clarity, lipid ligands are omitted from this top-view representation. (*E*) A Tyr151-Glu80 hydrogen bond prevents spacer protrusion in the SGL12-loaded structure. The $2F_o$-$F_c$ map (1.0 σ contour) is represented as a green mesh for side-chain atoms of Tyr151 and Glu80, in blue for ligand atoms. The interatomic distance between the two closest oxygens from Tyr151 and Glu80 is indicated. (*F*) Similar representation to that of *E* prepared using data from the crystal structure of shCD1b–PC–UL. PC atoms are colored exactly as SGL12 atoms in *B*, and with phosphorus in orange.

polar groups of anchored ligands, which might be required to facilitate the presentation of antigens with a range of polar heads.

**Antigen Binding Induces Conformational Changes in CD1b.** Remarkably, the presence of SGL12 was accompanied by an important shift toward the α1-helix of backbone and side-chain atoms of residues 149–152 that connect two helical segments of the α2-domain (Fig. 2*D*). The rmsd of backbone atoms from these four residues in copy A compared with their position in natively folded shCD1b was 2.4 Å (20). In contrast, the conformation of these residues in copy B, in shCD1b and in other published CD1b structures (6, 22), was essentially identical (rmsd below 0.6 Å). The displacement in the SGL12-loaded copy resulted in the establishment of a hydrogen bond between the Glu80 side-chain carboxylate and the Tyr151 hydroxyl group (Fig. 2 *D* and *E*). The interatomic distance between the two closest oxygen atoms from each residue decreased from 5.9 Å in natively folded shCD1b (Fig. 2*F*) to 2.6 Å in the SGL12-loaded copy. Accompanying these movements, the side-chain of Gln152 oriented toward the TCR-contacting interface, compared with other published structures (6, 20, 22), suggesting that this residue might play a role in modulating the interaction with TCR.

The conformational change of residues 149–152 had important structural consequences. It occluded the F′ pocket entrance, preventing spacer egress toward the TCR contacting surface. Compared with unloaded shCD1b, spacers repositioned by the length of at least 6 methylene units toward the A′ pocket in copy A, clearing above the F′ pocket the necessary space to accommodate the SGL12 sulfated glucose (compare Fig. 2 *E* and *F*). The groove volume decreased from approximately 2,400 $Å^3$ in natively folded shCD1b to <2,200 $Å^3$ in the presence of SGL12. Overall, this conformational rearrangement appears incompatible with full embedding of the SGL12 phthioceranoyl-like tail inside the A′ pocket and thus forces its methyl-branched motif to remain exposed above the CD1b surface.

**Influence of CD1b Conformational Dhanges on T-Cell Stimulation.** To investigate whether such groove structural reorganization is important for $Ac_2$SGL/SGL12 presentation to T cells, we evaluated T-cell responses using CD1b with Ala point mutations at residues Glu80 or Tyr151 (implicated in F′ pocket closure) or at Gln152 (residue that flipped toward the TCR in copy A). Stably transfected C1R cells expressing matched surface levels of wild-type and mutant CD1b were selected (Fig. 3*A*), and their capacities to activate the $Ac_2$SGL-specific T cells were evaluated (Fig. 3*B*).

Replacement of Glu80 or Tyr151 with Ala fully abrogated T-cell responses to $Ac_2$SGL and SGL12, supporting the importance of the conformational changes observed in the CD1b–SGL12–UL structure for productive $Ac_2$SGL presentation. Differently from E80A and Y151A, the Q152A mutation resulted in increased T-cell responses to $Ac_2$SGL and SGL12 at all antigen doses. Enhanced cytokine secretion at saturating $Ac_2$SGL doses argued against differences in the number of antigenic complexes displayed by Q152A CD1b at the APC surface, compared with wild-type CD1b, and suggested that complexes with stronger stimulatory capacity were formed. These results collectively indicate that the conformational changes of CD1b residues 149–152 control T-cell responses to $Ac_2$SGL antigens.

## Discussion

CD1b presents a remarkable variety of (glyco)lipids to T cells (1, 3). Previous structural studies described the intricacy of the

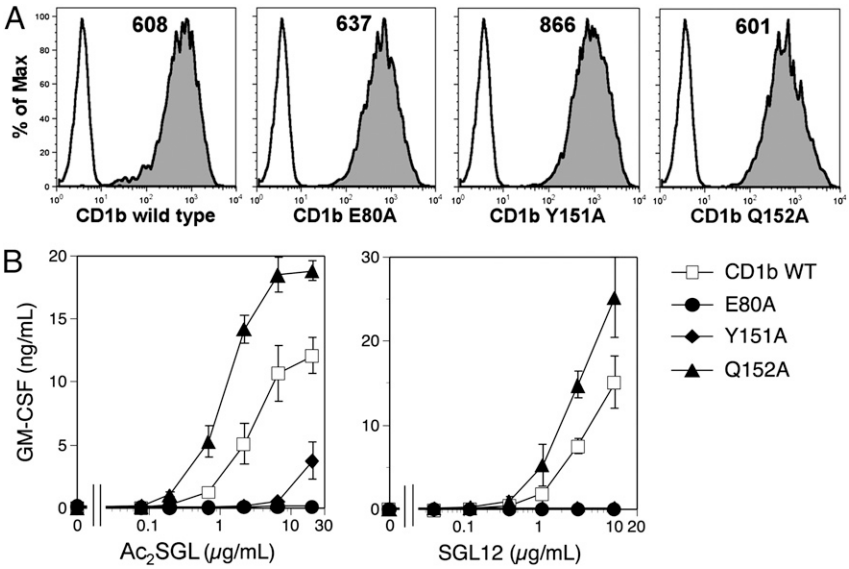


**Fig. 3.** Mutation of amino acids that change conformation upon antigen binding affects antigen presentation. (*A*) CD1b surface levels on C1R cells expressing wild-type or mutant CD1b, stained with anti-CD1b (gray histograms) or isotype control (white histograms) antibodies. Numbers indicate mean fluorescence intensity. (*B*) Stimulation of the Z4B27 T-cell clone with $Ac_2SGL$ or SGL12 presented by C1R cells expressing wild-type or mutant CD1b molecules. GM-CSF secretion is illustrated as mean of duplicates ± SD. Results are representative of at least two independent experiments.

CD1b groove (6, 20, 22), providing initial hints as to the mechanism of CD1b adaptation to lipid antigen. A detailed comprehension could not be attained because crystallized complexes were refolded in the presence of lipids and detergent, and the latter coincidentally occupied major portions of the T′ and F′ pockets (6), and also because the T-cell–stimulatory potential of the in vitro-refolded complexes was not assessed.

The data presented herein were obtained from a CD1b–antigen complex prepared from natively folded protein and having T-cell-stimulatory activity. A major finding was that CD1b presents $Ac_2SGL$ antigens to T cells with the participation of endogenous spacers. Our structural investigations indicated that spacers are 1,2- and 1,3-diacyl- and alkylacyl-glycerols, which are abundant components of cellular lipids (30). This ligand seemed to play an unpredicted functional role. In the presence of SGL12 and constrained by F′ pocket closing, spacers repositioned within the F′-T′-A′ superchannel toward the A′ pocket, compared with its position in unloaded shCD1b. Such movement not only allowed the accommodation of the bulky antigen polar head but also reduced the capacity of the A′ pocket for the SGL12 tail. This can be stated regardless of the length heterogeneity of spacers ($C_{36–44}$ or $C_{37–45}$ for 1,2- or 1,3-diradylGro, respectively), because (*i*) no mass differences were noted between spacer species dissociating from shCD1b–PC–UL and shCD1b–SGL12–UL complexes, and (*ii*) because F′ closing unambiguously blocks spacer egress in the SGL12-loaded structure. Considering that the A′-T′-F′ superchannel has the potential to accommodate approximately $C_{56–60}$-long tails (6) and that the mean spacer length is $C_{40}$, the repositioning of the latter is assumed to cause exposition of the methyl-ramified portion of the $C_{24}$-long tail of SGL12. Such possibility would explain why methyl ramifications in $Ac_2SGL$ and SGL are essential for antigenicity (17).

Binding of SGL12 to shCD1b was accompanied by conformational changes of residues 149–152 that brought closer the α1 and α2 helices and shut the F′ pocket entrance. Supporting the functional importance of these alterations, both E80A and Y151A CD1b mutants failed to elicit T-cell responses to $Ac_2SGL$/SGL12. Although still compatible with two residues that coincidentally contacted the $Ac_2SGL$-specific TCR, our combined functional and structural data rather suggest that Glu80 and Tyr151 are important because they sustain F′ closure and spacer displacement, alterations that would be mandatory for presentation of diacylsulfoglycolipids. Interestingly, F′ closure implicating the same two residues has been observed in the crystal structure of bovine CD1b3 (31). Such mechanism of groove tailoring to ligand structure thus differed from a proposed mechanism involving an alternate side-chain conformation of Phe84 (6).

Among residues 149–152, the Gln152 residue underwent a remarkable revolution of approximately 90° in the presence of SGL12 and adopted a position pointing toward the TCR. Indeed, residues 149–152 are at the most protruding region above the CD1b lipid-binding cleft. Any rearrangement of their conformation is expected to impact recognition by T cells. This was proven by the considerably stronger T-cell responses elicited with the CD1b Q152A mutant compared with wild-type CD1b. Further experimentation will be required to explore the role of Gln152 in restraining T-cell responses. Interestingly, a similar rearrangement of α2 interhelical residues of HLA-A2 was also noted in the crystal structure of a ternary complex HLA-A2/peptide/TCR (32). The conformation of residues Ala150-Val152 was found to switch in the face of the same TCR depending on the identity of the antigenic peptide, highlighting a mechanism whereby the antigen tuned the dynamic properties of the MHC molecule, and ultimately of the TCR, and facilitated cross-reactivity. Similarly, the flexibility of that interhelical segment could be exploited in CD1b as a means to further expand the structural diversity of antigens presented to T cells.

An intriguing question is how the structural reorganization of the SGL12-occupied groove was triggered (20). F′ closure and spacer repositioning might be consequence of the PC/antigen exchange process. Concomitant with PC discharge, spacers are predicted to slide within the groove to stabilize emptied portions. The Tyr151 would then interact with Glu80, thus closing the F′ entrance, a mechanism that could serve to prevent insertion of lipid tails into the F′ pocket. Eventually, spacer displacement might be reinforced by strong hydrogen bonds between diradylGro molecules and CD1b groove residues (Fig. S3). Short-tailed antigens would then bind to A′ and C′ pockets in combination with fully embedded spacers. The mentioned Glu80-Tyr151 and spacer-CD1b hydrogen bonds would contribute to retain exposed above the A' pocket medium-sized tails like those from $Ac_2SGL$. Conversely, these bonds would break and spacers would be expelled for presentation of *Mtb* MA, GMM, or GroMM.

In conclusion, this study revealed several unique structural features that confer CD1b with unusual pocket plasticity. These include an intricate pocket design, the presence of a repositionable spacer, the rearrangement of key residues affecting TCR recognition, and the ability to switch from an open to closed state the main entrance toward the F′ pocket and the C′ portal. Altogether, these features endow CD1b with an extraordinary

flexibility in adapting to foreign antigens, thus facilitating lipid antigen recognition and antimicrobial immune responses.

## Methods

Reagents, cell lines, the preparation of APC transfectants, T-cell activation assays, and other experimental details are described in *SI Methods*.

**Native Nano ESI Mass Spectrometry.** Recombinant shCD1b loaded with SGL12 was purified by chromatofocusing on a MonoP column (GE Healthcare) using a pH gradient between 6.5 and 4.0. Enriched CD1b–SGL12 complex was recovered as second eluting peak, concentrated, and buffer-exchanged against 10 mM Na acetate, pH 5.0. The last 18 residues belonging to the BirA extension tag were then removed by incubation of CD1b–SGL12 with LysC endoproteinase (Roche) (200:1 weight ratio) at 30 °C for 6 h, in 25 mM Tris/5 mM EDTA, pH 8.5. Details concerning the analysis by n-MS are given in *SI Methods*.

**Extraction of the Endogenous Spacer from shCD1b.** Recombinant shCD1b (2 mg) was immunopurified as previously described (20), with modifications. After PBS, column wash was continued with deionized water (30 mL), and the protein was eluted with aqueous acetic acid (25 mL, 0.2 M, pH 2.6) and collected in glass tubes. After pH neutralization with ammonium hydroxide (30%), pooled fractions were concentrated under vacuum to 1 to 2 mL and treated overnight at 30 °C with proteinase K (20 U, from *Tritirachium album*; Sigma). Lipids were extracted by three successive steps with PE (HPLC grade, 2 mL per step). Upper organic phases were pooled and dried. The aqueous phase was flowed with $N_2$ to remove remaining PE, and extraction was pursued with 2 × 2 mL of $CHCl_3$ (HPLC grade). The bottom phases were pooled and dried.

**Analysis by FT-ICR MS.** Protein ligands extracted with PE or $CHCl_3$ were analyzed by ESI FT-ICR MS, using a hybrid APEX Qe Instrument (Bruker Daltonics) equipped with an actively shielded 7-T magnet and a dual ESI source. Mass spectra were acquired in the positive-ion mode using standard experimental sequences as provided by the manufacturer. Samples were dissolved in a 50:50:0.03 (vol/vol/vol) mixture of 2-propanol/water/AA (30 mM) at pH 4.5 and sprayed at a flow rate of 2 μL/min. Capillary entrance voltage was set to 3.8 kV and drying gas temperature to 200 °C. Mass scale calibration was performed externally and controlled internally with compounds of known structure assuring a mass accuracy below 3 ppm.

**Thin-Layer Chromatography.** Silica gel TLC plates (SIL G/$UV_{254}$ 0.20 mm, 10 cm high; Macherey-Nagel) were prewashed by running successively to 9 cm first with $CHCl_3$/MeOH (9:1, vol/vol) and second with PE/$Et_2O$ (15:5, vol/vol). After the plate dried, samples (1–4 μg) were loaded and developed with PE/$Et_2O$/acetic acid (15:5:0.2, vol/vol/vol) to 8 cm. For visualization, the plates were dipped into 10% cupric sulfate in MeOH containing 4% phosphoric acid and 4% sulfuric acid, before being charred at 180 °C for 10 min.

**Crystallization of the Glycosylated shCD1b–SGL12–UL Complex.** Mouse-expressed shCD1b was loaded with SGL12 (*SI Methods*). After pH neutralization, the protein was purified by anion-exchange chromatography (Bio-Scale Q2 column; Bio-Rad) using a linear gradient from buffer A (10 mM Bis-Tris/1 mM EDTA/pH 6.5) to buffer B (500 mM NaCl in buffer A). The best crystals were grown after 1–3 d at 20 °C, using the hanging-drop vapor-diffusion method, from drops containing 1 μL shCD1b–SGL12 (5 mg/mL in 10 mM Bis-Tris/30–50 mM NaCl/1 mM EDTA/pH 6.5) and 1.0 μL precipitant [1.9 M $(NH_4)_2SO_4$, 0.2 M $NH_4Ac$, pH 6.6)]. Experimental details concerning X-ray data collection, structure determination, analysis and presentation are given in *SI Methods*.

**ACKNOWLEDGMENTS.** We thank Dr. Dominique Lafont [Institut de Chimie et Biochimie Moléculaires et Supramoléculaires, Centre National de la Recherche Scientifique (CNRS)] and Prof. Gudmundur G. Haraldsson (University of Iceland) for kindly providing synthetic lipids; Professors Raphael A. Zoeller (Boston University School of Medicine), Howard Goldfine (University of Pennsylvania), David A. Ford (St. Louis University), Robert C. Murphy (University of Colorado), and Joseph A. Laszlo (National Center for Agricultural Utilization Research) for enriching discussions; the European Synchrotron Radiation Facility staff (Grenoble, France) for excellent data collection facilities; Stefano Vavassori and Paula Cullen for reading the manuscript; and Olivier Saurel (IPBS, CNRS) for acquisition of $^1$H NMR data (spectrometers financed by the CNRS, Université Paul Sabatier, Région Midi-Pyrénées, and European Regional Development Fund). This work benefits from constant support of the CNRS, the European Union (FP6 TB-VAC program), the Agence Nationale de la Recherche Emergence (ANR-07-EMPB-029-01, France), and of the Swiss National Foundation (Grant 3100AO-122464/1). S. A.P. receives support from National Institutes of Health/National Institute of Allergy and Infectious Diseases Grant AI45889.

1. De Libero G, Mori L (2005) Recognition of lipid antigens by T cells. *Nat Rev Immunol* 5:485–496.
2. McFarland BJ, Beeson C (2002) Binding interactions between peptides and proteins of the class II major histocompatibility complex. *Med Res Rev* 22:168–203.
3. Barral DC, Brenner MB (2007) CD1 antigen presentation: How it works. *Nat Rev Immunol* 7:929–941.
4. Silk JD, Salio M, Brown J, Jones EY, Cerundolo V (2008) Structural and functional aspects of lipid binding by CD1 molecules. *Annu Rev Cell Dev Biol* 24:369–395.
5. McCarthy C, et al. (2007) The length of lipids bound to human CD1d molecules modulates the affinity of NKT cell TCR and the threshold of NKT cell activation. *J Exp Med* 204:1131–1144.
6. Gadola SD, et al. (2002) Structure of human CD1b with bound ligands at 2.3 A, a maze for alkyl chains. *Nat Immunol* 3:721–726.
7. Sieling PA, et al. (1995) CD1-restricted T cell recognition of microbial lipoglycan antigens. *Science* 269:227–230.
8. Gilleron M, et al. (2001) Acylation state of the phosphatidylinositol mannosides from *Mycobacterium bovis* bacillus Calmette Guérin and ability to induce granuloma and recruit natural killer T cells. *J Biol Chem* 276:34896–34904.
9. de la Salle H, et al. (2005) Assistance of microbial glycolipid antigen processing by CD1e. *Science* 310:1321–1324.
10. Gilleron M, et al. (2004) Diacylated sulfoglycolipids are novel mycobacterial antigens stimulating CD1-restricted T cells during infection with *Mycobacterium tuberculosis*. *J Exp Med* 199:649–659.
11. Beckman EM, et al. (1994) Recognition of a lipid antigen by CD1-restricted alpha beta+ T cells. *Nature* 372:691–694.
12. Layre E, et al. (2009) Mycolic acids constitute a scaffold for mycobacterial lipid antigens stimulating CD1-restricted T cells. *Chem Biol* 16:82–92.
13. Moody DB, et al. (1997) Structural requirements for glycolipid antigen recognition by CD1b-restricted T cells. *Science* 278:283–286.
14. Shamshiev A, et al. (2000) The alphabeta T cell response to self-glycolipids shows a novel mechanism of CD1b loading and a requirement for complex oligosaccharides. *Immunity* 13:255–264.
15. Shamshiev A, et al. (2002) Presentation of the same glycolipid by different CD1 molecules. *J Exp Med* 195:1013–1021.
16. de Jong A, et al. (2007) CD1c presentation of synthetic glycolipid antigens with foreign alkyl branching motifs. *Chem Biol* 14:1232–1242.
17. Guiard J, et al. (2009) Fatty acyl structures of mycobacterium tuberculosis sulfoglycolipid govern T cell response. *J Immunol* 182:7030–7037.
18. Cheng TY, et al. (2006) Role of lipid trimming and CD1 groove size in cellular antigen presentation. *EMBO J* 25:2989–2999.
19. Heck AJ (2008) Native mass spectrometry: A bridge between interactomics and structural biology. *Nat Methods* 5:927–933.
20. Garcia-Alles LF, et al. (2006) Endogenous phosphatidylcholine and a long spacer ligand stabilize the lipid-binding groove of CD1b. *EMBO J* 25:3684–3692.
21. Benesch JL, Ruotolo BT, Simmons DA, Robinson CV (2007) Protein complexes in the gas phase: Technology for structural genomics and proteomics. *Chem Rev* 107: 3544–3567.
22. Batuwangala T, et al. (2004) The crystal structure of human CD1b with a bound bacterial glycolipid. *J Immunol* 172:2382–2388.
23. Zajonc DM, Ainge GD, Painter GF, Severn WB, Wilson IA (2006) Structural characterization of mycobacterial phosphatidylinositol mannoside binding to mouse CD1d. *J Immunol* 177:4577–4583.
24. Zajonc DM, et al. (2005) Structure and function of a potent agonist for the semi-invariant natural killer T cell receptor. *Nat Immunol* 6:810–818.
25. Zajonc DM, et al. (2005) Structural basis for CD1d presentation of a sulfatide derived from myelin and its implications for autoimmunity. *J Exp Med* 202:1517–1526.
26. Zajonc DM, Savage PB, Bendelac A, Wilson IA, Teyton L (2008) Crystal structures of mouse CD1d-iGb3 complex and its cognate Valpha14 T cell receptor suggest a model for dual recognition of foreign and self glycolipids. *J Mol Biol* 377:1104–1116.
27. Koch M, et al. (2005) The crystal structure of human CD1d with and without alpha-galactosylceramide. *Nat Immunol* 6:819–826.
28. Giabbai B, et al. (2005) Crystal structure of mouse CD1d bound to the self ligand phosphatidylcholine: a molecular basis for NKT cell activation. *J Immunol* 175: 977–984.
29. Zajonc DM, Elsliger MA, Teyton L, Wilson IA (2003) Crystal structure of CD1a in complex with a sulfatide self antigen at a resolution of 2.15 A. *Nat Immunol* 4: 808–815.
30. Jones DR, Pettitt TR, Sanjuán MA, Mérida I, Wakelam MJ (1999) Interleukin-2 causes an increase in saturated/monounsaturated phosphatidic acid derived from 1,2-diacylglycerol and 1-O-alkyl-2-acylglycerol. *J Biol Chem* 274:16846–16852.
31. Girardi E, et al. (2010) Crystal structure of bovine CD1b3 with endogenously bound ligands. *J Immunol* 185:376–386.
32. Borbulevych OY, et al. (2009) T cell receptor cross-reactivity directed by antigen-dependent tuning of peptide-MHC molecular flexibility. *Immunity* 31:885–896.